SURFACE FEMTOCHEMISTRY OF OXYGEN AND COADSORBATES ON Pt(111)

R.J. FINLAY, T.-H. HER, C. WU, E. MAZUR
Gordon McKay Laboratory, Harvard University
9 Oxford Street, Cambridge, MA 02138

We review the photoprocesses of oxygen on Pt(111), both with and without coadsorbates, and recent progress in describing these processes. We present new data that address the chemical pathway to formation of CO_2 in $CO/O_2/Pt(111)$ induced by subpicosecond laser pulses. The data show conclusively that the O_2 desorbs molecularly. We also find that if the CO reacts by an atomic pathway then the capture of oxygen atoms by the CO is highly efficient; if it reacts by a molecular pathway then the oxygen atoms in the transition state are inequivalent.

1. Introduction

The surface chemistry of oxygen on transition metals has practical importance. For example, the oxidation of ethylene is catalyzed by transition metals. Although obtaining practical reaction rates requires placing the catalyst at high temperature and at a relatively high background pressure of reactants, studies under low-temperature, ultrahigh vacuum conditions further our understanding of these reactions. For example, studies under ultrahigh vacuum conditions reveal that at low temperature ($\approx$100 K) the O–O bond in an oxygen molecule that is chemisorbed on platinum is stretched compared to its length in the gas phase, and that π^* orbitals, which are anti-bonding with respect to the O–O bond, are occupied. At high temperatures, oxygen dissociates on transition metal surfaces; at low temperatures, the oxygen is, so to speak, captured for study on its way to dissociation. Similarly, studies of the exchange of charge between adsorbate and substrate, of the excitation and relaxation of adsorbate vibrations, and of surface bond configurations help advance our understanding of the reactions that occur in industrial applications.

The first photo-induced bimolecular reaction on a metal surface was discovered only in 1989.[1] Visible light was found to induce oxidation of carbon monoxide on $CO/O_2/Pt(111)$. Before this discovery, it was presumed that photo-induced reactions on a metal surface would be inhibited due to the strong quenching of the electronic and vibrational excitation of adsorbates on metals. However, the light can be absorbed in

the substrate, creating free carriers that interact with the adsorbate and then induce a reaction. The short absorption depth of visible photons in a metal (≈10 nm) concentrates the free carriers near the adsorbates. In addition, chemisorbed reagents are aligned in well-defined orientations, potentially allowing for direct coupling of the light with an adsorbate transition dipole. Since the discovery of the photo-induced oxidation of carbon monoxide on platinum in 1989, the photochemistry of adsorbates on metals, and in particular oxygen on transition metals, has become a very active field of research.[2]

After nearly a decade of research, many fundamental questions still remain unanswered. For example, in the production of CO_2 from $CO/O_2/Pt(111)$, is the CO_2 produced by a reaction between CO and an oxygen molecule or between CO and an oxygen atom created by photodissociation? Does the light directly excite the oxygen-platinum complex, or does it create a hot carrier in the substrate that causes chemistry through attachment to an adsorbate? How do these phenomena change when the photo excitation is a subpicosecond laser pulse instead of continuous wave (cw) illumination from a lamp? This paper summarizes recent studies of these issues. In addition, we present new experimental results that address the pathways to CO oxidation and O_2 desorption under subpicosecond laser irradiation, and experiments that address the nature of the electronic excitation leading to reaction.

In reactions induced by light pulses of nanosecond or longer duration, the product yield is found to scale linearly with incident fluence (energy per unit area).[3] The yield is linear because each photon excites a single electron that influences the adsorbates independently of any other photo-excited carriers. Section 2 summarizes the linear photochemistry of $O_2/Pt(111)$ and Section 3 that of oxygen and coadsorbates on platinum, focusing primarily on the oxidation of carbon monoxide.

For subpicosecond laser pulses, the pulse duration is shorter than both the coupling time between adsorbate vibrations and the substrate as well as the phonon-electron relaxation time in the metal. For such pulses the desorption yield is nonlinear with the number of incident photons.[4] In Section 4 we review the general characteristics of subpicosecond surface photochemistry. Section 5 presents the results of new experiments on the CO oxidation induced with subpicosecond laser pulses in $CO/O_2/Pt(111)$.

For a general introduction to surface photochemistry and ultrafast surface dynamics, the reader is referred to a recent book on this subject.[5] A number of papers [2,6-10] provide additional information on surface photochemistry and on the interactions of substrate electrons and adsorbates, complementing the information in this review.

2. Linear photochemistry of O2/Pt(111)

We begin by reviewing the bonding of oxygen to platinum, and then summarize experiments that aim to determine the nature of the interaction between the light and molecular oxygen that is chemisorbed onto a Pt(111) surface.

2.1 Oxygen on Pt(111)

Oxygen chemisorbs molecularly on Pt(111) at temperatures below 130 K; for temperatures below 30 K, oxygen is physisorbed. Physisorbed O_2 may be converted to chemisorbed O_2 by a brief anneal to 80 K.[11] The chemisorbed oxygen coverage saturates at 0.44 ML (1 ML = 1.49×10^{15} cm^{-2}, corresponding to one adsorbed species per platinum surface atom), with a $(3/2 \times 3/2)R15°$ low-energy electron diffraction (LEED) pattern.[12] We will denote chemisorbed oxygen by O_2/Pt(111).

Molecular oxygen has 12 valence electrons occupying the $2\sigma_g$, $2\sigma_u^*$, $1\pi_u$, $3\sigma_g$, and $1\pi_g^*$ orbitals.[13] In the gas phase, the π orbitals are two-fold degenerate. With O_2 adsorbed on the surface, the symmetry is reduced, lifting the degeneracy of the π orbitals. The $1\pi^*$ orbitals perpendicular to the surface hybridize with the platinum *d*-band, while the $1\pi^*$ orbitals parallel to the surface are not greatly perturbed.[14] Figure X.1 shows the energies of these orbitals for gas phase and for chemisorbed O_2. The approximate energies and widths of the states shown in Fig. X.1 are determined experimentally using ultraviolet photo-electron spectroscopy[15] and near-edge x-ray absorption fine-structure spectroscopy,[14,16] and in several theoretical treatments.[17-19]

The bonding of O_2 to the surface is due to electron transfer from the substrate to the π^* orbitals. The charge transfer increases the work function (5.8 eV for clean Pt(111)[20]) by 0.8 eV.[21] The amount of charge that the O_2 receives from the surface determines whether the O_2 is a peroxo (O_2^{2-}) or superoxo (O_2^{1-}) species. The peroxo species has a weaker O–O bond than the superoxo species because π^* is anti-bonding with respect to the O–O bond.

Electron energy loss spectra of oxygen on platinum show two O–O vibrations at 690 cm^{-1} and 870 cm^{-1}. These vibrations have been attributed to an atop species with O–O bond order 1, and a bridge-bonded species with O–O bond order below 1, respectively.[12,22] The 870 cm^{-1} O–O frequency is similar to that observed in peroxo dioxygen-metal complexes,[23] suggesting that the O_2 on Pt(111) is a peroxo

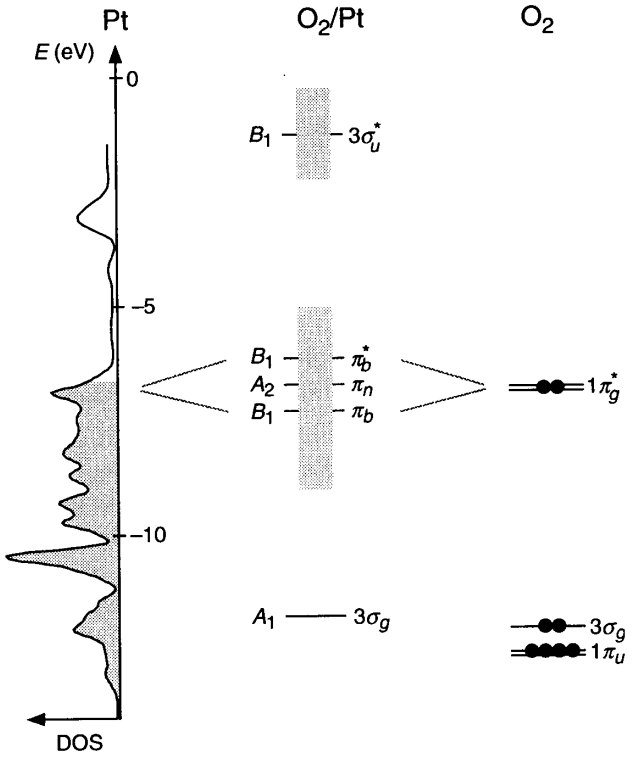

Figure X.1. Approximate electronic states of O_2/Pt(111). The calculated bulk density of states of platinum is plotted on the left, with the filled states below the Fermi level shaded.[24] The ground state configuration of gas phase O_2 is represented on the right.[13] The $1\pi_g^*$ orbital is antibonding with respect to the O–O bond.[13] The $3\sigma_u$ and $2\sigma_u$ and $2\sigma_g$ orbitals of O_2 are out of the energy range shown. Symmetries within the C_{2v} class are indicated. The component of $1\pi_g^*$ normal to the surface mixes with the platinum *d*-band forming bonding (π_b) and antibonding (π_b^*) orbitals with respect to the surface. The $1\pi_g^*$ orbital parallel to the surface remains non bonding (π_n). These three π orbitals are all anti-bonding with respect to the O–O bond; their occupation accounts for the lengthening of the O–O bond.[14,15] Vertical shaded bars indicate the approximate width of the $3\sigma_u^*$ orbital from near-edge x-ray absorption fine-structure spectroscopy[14] and the extent of the entire π_b and π_n region from photo-emission spectroscopy.[15]

species.[21] Other experiments, however, identify the oxygen as a superoxo species. For example, x-ray absorption studies of O_2/Pt(111) provide a value for the separation in energy between the 1σ and the $1\pi^*$ and $3\sigma^*$ orbitals.[14,16] From this energy separation, the O–O bond length of the adsorbed oxygen is determined to be 0.137 ±

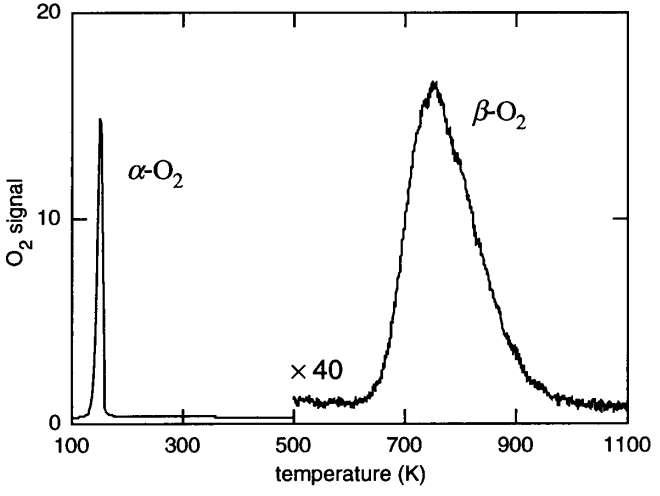

Figure X.2. Temperature programmed desorption of saturation O_2/Pt(111) obtained at a heating rate of 4 K/s. Oxygen desorbs molecularly at 145 K (α-O_2). Recombinative desorption occurs near 750 K (β-O_2).

0.005 nm,[14] compared to 0.1207 nm in the gas phase, consistent with superoxo O_2.[23] Ultraviolet photoelectron spectra and calculations support this interpretation.[15,19]

A surface layer of atomic oxygen on Pt(111) can be obtained by exposing the surface to molecular oxygen at a platinum temperature above 145 K. The surface coverage saturates at 0.25 ML with a p(2×2) LEED pattern.[21] The oxygen binds in fcc three-fold hollow sites,[25] giving rise to a 470-cm^{-1} Pt–O vibration. Higher coverages of atomic oxygen can be attained by photodissociation of N_2O/Pt(111),[26] or by electron-beam dissociation of O_2/Pt(111).[12]

2.2 Thermal chemistry

Figure X.2 shows a temperature programmed desorption (TPD) scan of a saturated[21] O_2/Pt(111) preparation. The feature at 145 K, denoted α-O_2, is due to desorption of intact molecules. Above this temperature the oxygen molecules dissociate leaving atomic oxygen behind on the surface. The broad feature at 750 K, denoted β-O_2, is due to desorption of molecules formed by the recombination of atoms at the surface.[27] From temperature programmed desorption experiments it follows that the binding

energy of O_2 is 0.4 eV and that of atomic oxygen is 1.1 eV at saturation coverage.[21]

The thermal dissociation of O_2 occurs preferentially at bridge sites.[12] At low coverage dissociation begins at 94 K, but at high coverage the dissociation pathway is inhibited until molecular desorption at 145 K has reduced the surface density.[22] The ratio of α-O_2 to β-O_2 therefore indicates the initial coverage: the lower the coverage, the more β-O_2 there is compared to α-O_2.[12]

2.3 Linear photochemistry of O_2/Pt(111)

Irradiation of O_2/Pt(111) with ultraviolet light causes desorption of oxygen molecules from the surface, dissociation of oxygen into atoms that remain on the surface, and rearrangement of oxygen molecules on the surface. The rates of desorption and dissociation have been measured as a function of photon energy, incident fluence, and angle of incidence.

The photo-induced desorption yield is measured with a mass spectrometer.[20,28] As the surface coverage decreases during irradiation, the mass spectrometer signal drops. The decay time of the signal allows one to determine the cross section for photo-induced desorption.[28] Another way to determine the cross section is to analyze the surface after irradiation with electron energy loss spectroscopy. The intensity of the spectral feature corresponding to Pt–O vibration at 470 cm^{-1} is a measure of the coverage of atomic oxygen and can be used to infer the extent of photo-induced dissociation of the oxygen. The intensities of the 690 and 870 cm^{-1} peaks indicate the coverage of molecular oxygen remaining on the surface.

Cross sections for photo-induced dissociation can be determined by performing a TPD scan after irradiation. The α-O_2 yield in a post-irradiation scan indicates how much molecular oxygen remains on the surface after irradiation and the ratio of α-O_2 to β-O_2 provides information on the photo-induced dissociation cross section. Unfortunately the analysis is complicated by the dissociation of molecular oxygen during the TPD scan — even without any photodissociation, β-O_2 appears in the TPD scan.

The α-O_2 peak in the post-irradiation TPD scan is broadened compared to the scan obtained from a surface without irradiation.[29,30] This suggests that a photo-induced rearrangement of the adsorbates has occurred. The nature of this rearrangement, however, is unknown.

Table X.1 summarizes the photo-induced desorption and dissociation cross sections for O_2/Pt(111) reported in the literature. Some authors extract two cross sections from each O_2 depletion curve.[20,31] The two cross sections could be due to two species on the surface with different photoactivity.[20]

2.4 Direct vs. indirect excitation

The photo-induced surface chemistry of O_2/Pt(111) has been attributed to both direct and indirect excitation mechanisms. Direct excitation occurs when the light induces an electronic transition within the adsorbate-substrate complex. When the excitation of the adsorbates is caused by photo-excited carriers in the substrate, the excitation is called indirect.

The dependence of the photo-induced yield on the angle of incidence can help distinguish between a direct or indirect mechanism. The efficiency of a direct transition depends on the angle between the electric field vector and the orientation of the transition dipole.[33] For an indirect mechanism, the dependence of yield on incidence angle results from the dependence of the absorption by the metal substrate on the incidence angle.[34] Calculations show a difference in dependence on incidence angle for the yield in direct and in indirect mechanisms when the transition dipole for the direct excitation is perpendicular to the surface.[18,33] However, if the transition dipole is parallel to the surface, then the angular dependencies of the direct and indirect mechanisms are similar.[33] Measurements of the yield as a function of the incidence angle of the light therefore can be used to check for a direct mechanism with a transition dipole normal to the surface, but are not useful when the transition dipole is parallel to the surface.

Figure X.3 shows how the dependence of yield on photon energy might help

$h\nu$ (eV)	cross section (10^{-24} m^2)			Reference
	dissociation	desorption	total	
3.5			8	[31]
3.7			3.3	[1]
3.9–5.4	5.7	12		[29]
4.0	1	6		[32]

Table X.1. Cross sections for linear photochemistry of O_2/Pt(111) at various photon energies. Refs. [1] and [31] report two decay constants; only the slower one is reported here.

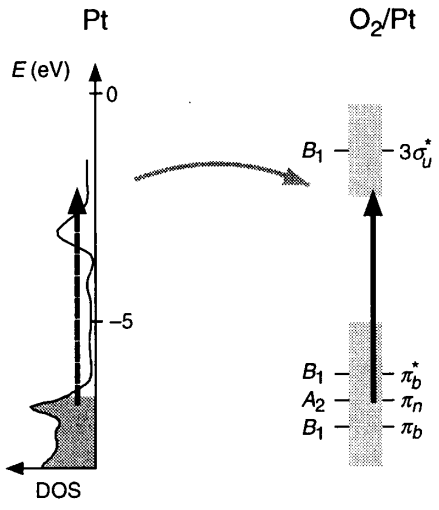

Figure X.3. Direct and indirect transitions mechanisms. The solid arrow represents a direct transition within the adsorbate-substrate complex. The dashed arrow represents excitation of a carrier in the substrate. This excitation produces a carrier that can transfer to the adsorbate (gray arrow).[35]

distinguish between direct and indirect excitation.[35] The solid vertical arrow represents a direct transition between electronic states of the adsorbate-substrate complex. The dashed arrow represents excitation of a carrier in the substrate; transfer of this carrier to the adsorbate is possible only if the carrier energy is comparable to that of an electronic state of the adsorbate. As the photon energy is increased, the onset of photochemistry is similar for the two excitation mechanisms if the initial state of the direct transition is near the Fermi level. For photon energies past the peak of the direct transition, however, direct excitation is no longer possible, whereas indirect excitation due to photo-excited carriers that have lost some of their initial excitation energy in the metal is still possible.

2.5 Direct versus indirect excitation—experimental evidence

There are considerable discrepancies in the interpretation of the published experimental data on the linear photo-excitation of O_2/Pt(111). One group reports that the cross section for O_2 desorption is non zero at normal incidence and that it increases towards glancing incidence.[36] They attribute the yield at normal incidence either to indirect

Threshold energy (eV)		Ref.
dissociation	desorption	
< 2.7	2.7	[1] ,[20]
4.2	2.7	[29]

Table X.2. Thresholds for linear photochemistry of O_2/Pt(111) obtained by post-irradiation electron energy loss spectroscopy.

excitation or to direct excitation of a transition dipole moment in the plane of the surface. On the other hand, the increase in yield with incidence angle must be attributed to a direct excitation with a transition dipole normal to the surface, because indirect excitations or direct transitions with a dipole in the surface plane do not increase much with incidence angle.[33]

Another group also studied the rate of desorption from O_2/Pt(111) as a function of the incidence angle of the light.[20] Because they were unable to obtain absolute efficiencies, the authors report the ratio of *p*-polarized to *s*-polarized photoyields as a function of incidence angle. The ratio increases with incidence angle from a value of one at normal incidence. For a direct excitation with a transition dipole normal to the surface there should be no yield at normal incidence. Furthermore, the calculated ratio of *p*-polarized to *s*-polarized photoyields increases more rapidly than observed experimentally. The authors therefore conclude that a direct transition due to a perpendicular transition dipole does not agree with the observed polarization dependence.

Table X.2 lists the observed thresholds for desorption and dissociation as a function of photon energy.[1,20,29] The disagreement over the photon energy threshold for photodissociation is unresolved.[20] The dependence of the cross sections for desorption and dissociation of O_2/Pt(111) on photon energy coincides with a feature in the electron energy loss spectrum of O_2/Pt(111) corresponding to an electronic transition in the O_2–Pt complex, suggesting that the O_2 desorption and dissociation are due to a direct transition.[20]

Experimental support for an indirect desorption mechanism is provided by measurement of the translational energy distribution of O_2 desorbed from O_2/Pt(111) during exposure of the surface to beams of O, H, and N atoms.[37] The O_2 desorbs with a bimodal energy distribution. The authors attribute the desorption to a local change in the charge distribution when an oxygen atom from a photodissociated oxygen molecule chemisorbs near another oxygen molecule. They also measured the translational energy distribution of oxygen molecules photodesorbed from O_2/Pt(111)

with cw irradiation. The translational energy distribution of the photodesorbed oxygen is similar to that observed atomic-beam-induced desorption of oxygen. This leads the authors to conclude that photodesorption of oxygen, too, is induced by the dissociation of a nearby oxygen molecule. This atomic-oxygen induced displacement mechanism reportedly also contributes to photodesorption of oxygen molecules from O_2/Pd(111), a system closely related to O_2/Pt(111).[38]

2.6 Identifying the relevant orbitals

Group theory identifies certain transitions in the O_2/Pt(111) complex that, due to their symmetries, are not coupled by an electric dipole and therefore can not be involved in direct excitation. Here, we briefly summarize a few results from group theory that help identify which orbitals can be responsible for direct excitation.

The O_2 molecule and the first layer of platinum atoms have C_{2v} symmetry.[13] The lower layers of the platinum further reduce the symmetry, but the platinum orbitals most relevant to transitions within the adsorbate-substrate complex are localized within the first layer. The C_{2v} class has four irreducible representations, denoted $\{A_1, A_2, B_1, B_2\}$ and each electronic state of O_2/Pt(111) transforms as one of these representations. The symmetry of each orbital is indicated in Fig. X.1. The z-axis is taken to lie along the surface normal, collinear with the C_2 symmetry axis; the x-axis lies along the O–O bond.

A transition between two states is possible if the symmetry of the transition dipole is the same as the symmetry of the direct product of the representations of the initial and final states.[13] Within the C_{2v} class, the components of the transition dipole vector transform as (B_1, B_2, A_1). Table X.3 gives the components of the transition dipole vector that couple states of each of the possible symmetries. For example, a transition dipole oriented along the x-axis couples states of symmetry $A_2 \leftrightarrow B_2$ or $A_1 \leftrightarrow B_1$.

C_{2v}	A_1	A_2	B_1	B_2
A_1	μ_z		μ_x	μ_y
A_2		μ_z	μ_y	μ_x
B_1	μ_x	μ_y	μ_z	
B_2	μ_y	μ_x		μ_z

Table X.3. Dipole allowed transitions in the C_{2v} symmetry class.

The conclusion[20] that the transition dipole cannot be normal to the surface eliminates from consideration the transitions along the diagonal of Table X.3. The direct transitions $3\sigma_g \rightarrow \pi^*$, $1\pi_{uz} \rightarrow \pi^*$, and $\pi_n \rightarrow 3\sigma_u^*$ have appropriate symmetry for a transition dipole in the plane of the surface, and energies in rough agreement with the experimentally observed wavelength dependence.[20] Another group attributes dissociation to $\pi_n \rightarrow 3\sigma_u^*$ and desorption to $\pi_n \rightarrow \pi^*$ transitions.[29]

2.7 Summary

Both direct photo-induced transitions between orbitals within the O_2/Pt(111) complex, and indirect activation of the adsorbate by photo-excited substrate carriers have been proposed. Conflicting experimental data leave the issue unresolved. There is also evidence that desorption of an oxygen molecule can be induced by nearby chemisorption of an oxygen atom.

3. Linear photochemistry of coadsorbed systems on Pt(111)

When O_2 is coadsorbed with another species the photochemistry is more complex because, along with dissociation and desorption, reactions can occur between oxygen and the coadsorbate. In this section we review the oxygen–coadsorbate systems on platinum that are known to be photo-active.

3.1 Thermal chemistry of CO/O$_2$/Pt(111)

Oxygen and carbon monoxide can be coadsorbed on Pt(111) by exposing the surface below 130 K first to O_2 and then to CO. After carbon monoxide exposure, the intensity of the O–O vibration in electron energy loss spectra is reduced by a factor two,[20] indicating that the carbon monoxide displaces[39] about half the adsorbed oxygen molecules to the gas phase. The electron energy loss data show that the carbon monoxide molecules occupy only atop sites in the presence of preadsorbed molecular oxygen and that the CO coverage is 0.25–0.30 ML.[20]

Table X.4 summarizes the main features observed in a temperature programmed reaction scan of CO_2 from CO/O_2/Pt(111).[27,40] The features have been identified using angular-resolved temperature programmed reaction scans and time-of-flight

measurements at a wide range of reagent coverages. The CO_2 yields are attributed to reaction between CO and O under different spatial distributions.[40]

The α-CO_2 feature coincides in temperature with desorption and dissociation of oxygen on platinum. Using isotopic substitution it was shown that the α-CO_2 cannot be attributed to a reaction between carbon monoxide and an equilibrated oxygen atom from a dissociated oxygen molecule.[27] The CO must react with an oxygen atom before that atom equilibrates with the surface.

The three β-CO_2 peaks are attributed to reaction of carbon monoxide with thermalized atomic oxygen. The β_3-CO_2 results from reaction of the CO with oxygen atoms in a densely packed mixed layer of CO and O. As the sample temperature is increased and coverage drops, diffusion occurs; reactions during segregation into islands lead to the β_2-CO_2 feature. Once segregation is complete, reaction at the edges of the islands leads to β_1-CO_2.

When atomic, instead of molecular, oxygen is coadsorbed with carbon monoxide on Pt(111), the β_1 and β_2-CO_2 features appear, but not β_3-CO_2.[41] The absence of this feature is attributed to the lower coverage (0.25 ML) of atomic oxygen in CO/O/Pt(111) compared the 0.38-ML coverage achieved during thermal dissociation of oxygen in CO/O_2/Pt(111).[40]

3.2 Linear photochemistry of CO/O_2/Pt(111)

Several groups have studied the photochemistry of CO/O_2/Pt(111) induced with arc lamps[1,20,30] and nanosecond laser pulses[32]. All observe O_2 desorption and CO_2 formation using a mass spectrometer. The surface coverage after irradiation is determined with temperature programmed reaction scans.[30]

The results are analyzed in terms of three photo-induced processes: desorption and dissociation of molecular oxygen, and reaction between carbon monoxide and

feature	T(K)	proposed physical origin
α	145	reaction with energetic oxygen dissociation fragments
β_3	200	reaction in high-density mixed layers of CO and O
β_2	250	reaction during segregation of CO and O
β_1	330	reaction at island edges and 2-D gas interactions

Table X.4: Interpretation of the features observed in temperature programmed reaction scans of CO/O_2/Pt(111) after Ref.[40].

oxygen:[30]

$$h\nu + O_2\,(ad) \rightarrow O_2\,(g)$$
$$h\nu + O_2\,(ad) \rightarrow 2\,O\,(ad)$$
$$h\nu + O_2\,(ad) + CO\,(ad) \rightarrow CO_2\,(g) + O\,(ad)$$

The yield of each process depends on a cross section (σ_{des}, σ_{diss}, or σ_{rxn}), the photon flux (ϕ), and the coverage of O_2.[30] The authors show that the O_2 coverage decays exponentially with a rate constant $\phi\sigma_{tot}$, where $\sigma_{tot} \equiv \sigma_{des} + \sigma_{diss} + \sigma_{rxn}$. For this reason, the desorption and reaction depletion curves decay exponentially with a rate constant $\phi\sigma_{tot}$. Table X.5 summarizes the reported cross-sections for CO/O_2/Pt(111).

3.3 Mechanism for linear photo-oxidation of CO

Two mechanisms have been proposed to explain the photo-induced reaction of CO in CO/O_2/Pt(111). In the hot atom mechanism, the CO reacts with an excited atom fragment from a dissociated oxygen molecule.[20] In the molecular mechanism, the CO reacts with an intact O_2 molecule.[32]

One group argues in favor of the molecular pathway by comparing the cross sections for O_2 dissociation and for CO reaction.[32] Their data indicate that the CO reaction cross section is 100 times larger than that for O_2 dissociation. (Tables X.1 and X.5). This implies there is insufficient dissociation and consequently insufficient oxygen atoms to account for the observed CO_2 yield, and so the authors attribute CO reaction to the molecular mechanism.[32] In contrast, another group reports a dissociation cross section that is roughly ten times as large as the reaction cross section (Table X.5).[30] Though this does not prove that the CO reaction is due to the atomic mechanism, it does indicate that there is sufficient O_2 dissociation to make the atomic mechanism possible.

$h\nu$ (eV)	Cross section (10^{-24} m^2)				Ref.
	σ_{diss}	σ_{des}	σ_{rxn}	σ_{tot}	
4.0			100		[32]
4.0				8	[31],[30]
3.9–4.8	0.4	0.22	0.035	0.66	[30]

Table X.5. Cross-sections for linear photochemistry of CO/O_2/Pt(111).

3.4 Experimental evidence for hot oxygen atom processes on platinum

There are several photo-induced bimolecular reactions on Pt(111) that have been attributed to hot oxygen atoms. For example, under cw irradiation molecular oxygen desorbs from $H/O_2/Pt(111)$ at 85 K.[42] Electron energy loss spectroscopy following irradiation reveals the vibrational signatures of OH and H_2O on the surface. The authors propose that reaction proceeds by dissociation of oxygen molecules and capture of the atoms by hydrogen.

Production of O_2 and desorption of N_2 was observed when $N_2O/O/Pt(111)$ is irradiated with 193-nm laser pulses.[43] Isotopic labeling shows that the oxygen atom from the N_2O reacts with a preadsorbed oxygen atom. On the basis of the translational energy distributions of the N_2, the authors conclude that formation of O_2 results from a reaction between a preadsorbed oxygen atom and a dissociation fragment of N_2O, rather than a direct reaction with N_2O.

When xenon, krypton, or argon are coadsorbed with molecular oxygen on Pt(111) at 20 K, the noble gas atoms desorb with a distribution peaked 35° off the surface normal under ultraviolet irradiation.[44] The cross section for noble gas desorption is comparable to the cross sections for O_2 photodissociation. In contrast, no desorption of noble gas atoms occurs with physisorbed molecular oxygen (which does not photodissociate) or without coadsorbed oxygen. These observations suggest that the noble gas desorption is caused by an atomic oxygen fragment. The translational energy of the atomic oxygen fragment after dissociation may account for the angle at which the noble gases desorb.[44]

3.5 Experimental evidence for molecular oxygen processes

A photo-induced bimolecular reaction between N_2O and CO in $CO/N_2O/Pt(111)$ at 47 K has been observed.[45] The reaction was induced with an arc lamp using wavelengths in the range 230–1000 nm. During irradiation, CO_2 desorption is observed and in post-irradiation TPR scans CO_2 desorbs near 85 K. This feature at 85 K is due to desorption of CO_2 formed during irradiation of the sample. When irradiation is continued until the N_2O coverage is reduced to 55%, however, CO_2 appears in the TPR scans only near 270 K. This feature at 270 K is attributed to β-CO_2 produced by a thermal reaction between CO and atomic oxygen fragments from photodissociated N_2O.

If dissociation of N_2O is the first step in the formation of CO_2, it is unlikely that all the oxygen atoms produced are captured by carbon monoxide. The oxygen atoms that escape reaction should equilibrate with the surface and appear as β-CO_2 in post-irradiation temperature programmed reaction scans. However, the β-CO_2 is only observed following very long exposures. The authors therefore conclude that until the surface coverage is substantially reduced, CO oxidation occurs in a reaction process where the N–O bond breaking and O–C bond formation take place simultaneously. Such a process is called a concerted reaction.

4. Surface femtochemistry

The duration of subpicosecond laser pulses is shorter than the coupling of adsorbate-vibrational modes to the substrate, and the coupling of substrate electrons and phonons. The surface reactions induced with subpicosecond laser pulses differ markedly from the reactions under low-intensity irradiation. We will begin this section with a summary of the general properties of nonlinear surface femtochemistry.

4.1 General characteristics of surface femtochemistry

Subpicosecond laser-induced surface reactions have been observed in a variety of systems: desorption of NO from NO/Pd(111),[4,46] CO from CO/Cu(111)[4,47] and CO/Cu(100),[48] O_2 from O_2/Pt(111)[28,31,49] and O_2/Pd(111),[50] and both O_2 and CO_2 from CO/O_2/Pt(111).[28,31,49] Common features of these reactions include a nonlinear dependence of yield on fluence (see, *e.g.*, Fig. X.6), a high desorption and reaction efficiency, and highly excited non thermal internal state distributions.[4,46] In some cases the branching ratio between two products can be changed and photoactivity is observed at wavelengths for which there is no linear photochemistry.

4.2 Time scale for excitation and desorption

The time scale of the excitation governing desorption can be probed using two pulses separated by an adjustable delay. The total yield from both pulses is measured with a mass spectrometer as a function of the delay. Such two-pulse correlations have been obtained for NO desorption from NO/Pd(111),[51] for O_2 desorption from

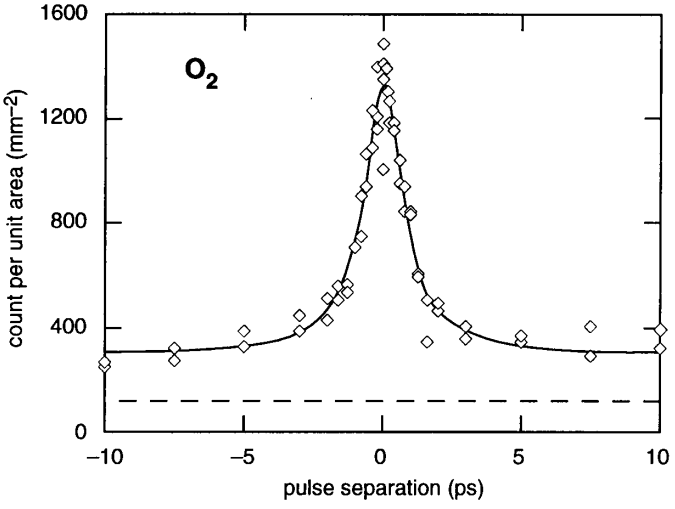

Figure X.4. Combined yields from two 70-fs laser pulses incident on O_2/Pt(111) at 90 K, from Ref. [28]. The FWHM of the central feature is 1.8 ps.

O_2/Pt(111),[28,52] and for CO from CO/Cu(100).[48] Figure X.4 shows a two-pulse correlation obtained with 70-fs pulses incident on O_2/Pt(111).[28] Each data point represents the total yield of desorbed O_2 induced by two time-delayed laser pulses incident at the same spot on the sample. The dashed line indicates the yield measured for the two pulses acting independently; the observed signal reaches this uncorrelated level in about 0.1 ns.[28] The 1.8-ps wide central peak shows the time interval over which the adsorbate-substrate system retains some excitation from the first pulse. The broad width of the autocorrelation compared to the 70-fs laser pulse duration, is generally considered proof that the excitation mechanism responsible for surface chemistry induced with subpicosecond pulses is indirect rather than direct.[51]

The time required for subpicosecond laser-induced desorption of CO from Cu(111) has been measured using surface second harmonic generation.[47] The instantaneous surface coverage of CO is determined from the second-harmonic conversion efficiency for a subpicosecond probe pulse; this efficiency depends on the coverage of CO. The surface is probed at successive time intervals following excitation of the surface with an intense subpicosecond pump pulse. The authors conclude that the CO desorption induced by the pump pulse is complete in less than 0.35 ps.[47]

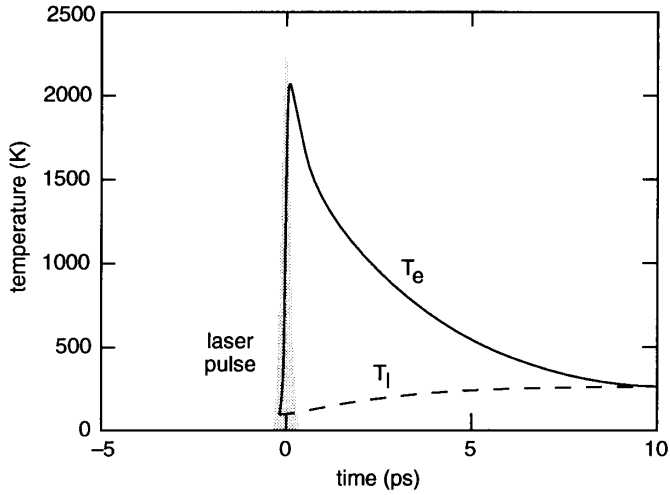

Figure X.5. Calculated evolution of electron and lattice temperatures following excitation of Pt with a 100-fs, 800-nm laser pulse of 32 $\mu J/mm^2$.

4.3 Electron and lattice temperatures under subpicosecond excitation

The interaction of a short laser pulse with a metal is described as follows. The photons excite electrons within the optical absorption depth of the metal. Within a few hundred femtoseconds the electrons come to thermal equilibrium while the lattice remains cold. The electrons diffuse in to the bulk of the crystal, and they couple to the lattice on a time scale of about a picosecond.

One can assign two separate temperatures to the electrons and lattice, and write two coupled equations for the evolution of these temperatures.[53] The equations are easily solved numerically. Figure X.5 shows the evolution of the electron and lattice temperatures at the surface of platinum under excitation by a 32 $\mu J/mm^2$, 800-nm pulse. Note the large transient rise in the surface electron temperature and the subsequent equilibration of the electron and lattice temperatures on a time scale of a few picoseconds. Although the calculation is subject to the limitations of the simple model and the difficulty of determining physical constants relevant at elevated temperatures, the general characteristics of Fig. X.5 have been confirmed experimentally for gold.[54,55]

4.4 Modeling surface femtochemistry

A number of models have been developed to account for the phenomena described in Section 4.1. All current models attribute the surface chemistry to the transient rise in surface electron temperature described in Section 4.4. The models range from purely phenomenological to explicit calculations of trajectories on realistic multi-dimensional potential energy surfaces. In this Section we provide only a brief survey.

The coupling between the substrate electrons and lattice and the vibrational modes of an adsorbate has been treated phenomenologically using a frictional model.[48] According to this model, the energy in the adsorbate vibration, U_v, depends on the energies in the electron and phonon modes as

$$\frac{dU_v}{dt} = \frac{U_e - U_v}{\tau_e} + \frac{U_p - U_v}{\tau_p} \tag{4}$$

where τ_e and τ_p describe the time scale for coupling of electrons and phonons to the CO vibration. The friction model successfully describes the width of the observed two-pulse correlation for CO from Cu(100) and the nonlinear relationship between the yield and fluence.

The excitation of the adsorbate is considered more explicitly in molecular dynamics calculations. The fundamental mechanism for these calculations is a change in the effective potential energy surface governing motion of the adsorbate caused by an electronic transition in an adsorbate-substrate complex or by charge transfer from the substrate to the adsorbate. The adsorbate moves on the new potential energy surface until the electronic excitation is quenched (by relaxation of the excitation in the adsorbate-substrate complex or by transfer of charge back to the surface). Following this excitation/de-excitation cycle the adsorbate is displaced from its original equilibrium position and may have sufficient translational and potential energy to desorb or react.[56-58] On metal surfaces the lifetime of an adsorbate electronic excitation is estimated to be no more than a few femtoseconds.[59] The short lifetime restricts the amount of time over which motion can occur on the upper potential energy surface and reduces reaction rates. For subpicosecond laser excitation, however, the adsorbates are exposed to a much higher density of excited substrate electrons and multiple excitation/de-excitation cycles can enhance reaction rates.[59] Although the excited state potential energy surfaces are not well known, molecular dynamics calculations account at least qualitatively for the properties of linear[60] and nonlinear[59] photochemistry.

Another approach combines the simplicity of the frictional coupling model with potential energy surfaces obtained from *ab-initio* calculations. For example, the subpicosecond laser-induced desorption of CO from Cu(100) has been modeled using a 108-atom model of a Cu(100) surface with adsorbed CO.[61] The motion of the CO is determined by adsorbate-substrate and adsorbate-adsorbate interaction potentials, by frictional coupling to the substrate electrons, and by impulsive stimulation from the substrate electrons. The model qualitatively accounts for the overall reaction yield, and the translational and internal energy of the desorbed CO.

4.5 Non thermal electron distributions

In the models discussed above, the electron distribution is always considered to be in thermal equilibrium. A current subject of debate, however, is whether the nonequilibrium electron distribution and its relaxation to a Fermi distribution need to be considered in desorption induced by subpicosecond laser pulses.[28,62] Indeed, recent studies of the electron distribution in a gold film following subpicosecond laser pulse excitation, provide evidence that the electron distribution is nonthermal for hundreds of femtoseconds.[63-65]

When an electron absorbs a photon, the energy it receives is very large compared to typical thermal energy scales. The subsequent relaxation of this electron towards the Fermi level has been described in two models.[35] The first model assumes relaxation by scattering of a photo-excited electron with an electron at the Fermi level, creating two excited electrons of equal energy.[35] The scattering processes continue in generations, with each generation producing twice the number of excited electrons. This model has been applied to describe the low-intensity photodesorption of NO/Pt(111).[66] A more sophisticated model uses Fermi liquid theory to describe the electron relaxation.[67] However, this model has not yet been applied to nonlinear surface femtochemistry.

5. Pathways to desorption and reaction in surface femtochemistry

Our own work has recently focused on the surface femtochemistry of CO/O_2/Pt(111).[28,49] Here we present new results of a study of the reaction and desorption pathways using isotopic labeling.

5.1 Experimental

The experiments were conducted on a 12-mm diameter Pt(111) crystal in an ultrahigh-vacuum chamber with a base pressure of 5×10^{-11} torr. Common contaminants of platinum are silicon, sulfur, phosphorous, and carbon. These are removed with Ne ion sputtering at an ion energy of 0.5 kV, annealing at 1100 K in vacuum and at 500–1000 K in a 10^{-8} torr background of oxygen.[68] Surface order is verified with LEED spectroscopy. Cleanliness is verified with Auger spectroscopy.[30]

After cleaning, various combinations of molecular oxygen, atomic oxygen, and carbon monoxide are adsorbed to saturation onto the platinum surface. Molecular oxygen is deposited directly after a cleaning cycle, as soon as the platinum temperature has fallen to 94 K. At this temperature there is no thermal dissociation of the oxygen. To coadsorb CO and O_2, carbon monoxide is deposited after the oxygen. A coverage of atomic oxygen is obtained by exposing the platinum surface to molecular oxygen at a surface temperature of 250 K.[21] The surface is then further cooled before depositing any coadsorbates.

Isotopic mixtures of $^{16}O_2$ and $^{18}O_2$ are prepared by mixing the isotopes outside the chamber and then depositing the isotopic mixture as in a regular O_2/Pt(111) preparation. To reduce background pressure while still obtaining saturation coverage, all adsorbates are deposited using a tube of 12 mm diameter that is brought to within 3 mm of the platinum surface. We verified the coverages using temperature programmed reaction spectroscopy and LEED. All laser experiments are performed at a base temperature of 84 K.

We studied the photochemistry of CO/O_2/Pt(111) using the frequency-tripled output of a regeneratively amplified Ti:Sapphire laser at 267 nm. The frequency-tripled output of the laser consists of a 1-kHz train of 0.24-ps pulses of up to 25 μJ per pulse. The pulse duration was determined by difference-frequency mixing the pulse with the 800-nm fundamental in a thin BBO crystal.[69] The energy of each laser pulse is measured with a calibrated photodiode. This energy reading is converted into absorbed fluence taking into account spatial profile, angle of incidence, platinum reflectivity, and absorption and reflection losses of the vacuum chamber windows. The fluence varies over the spatial profile of the laser spot; values quoted below refer to the local absorbed fluence at the peak of the spatial profile.

For each laser pulse, the reaction yield at one mass-to-charge ratio is measured with a quadrupole mass spectrometer. The mass spectrometer has a tube with an inner diameter of 4 mm that extends from the ionizer to the sample. Nearly the entire solid angle at the opening of the tube is filled by the Pt(111) crystal. Using a high-speed

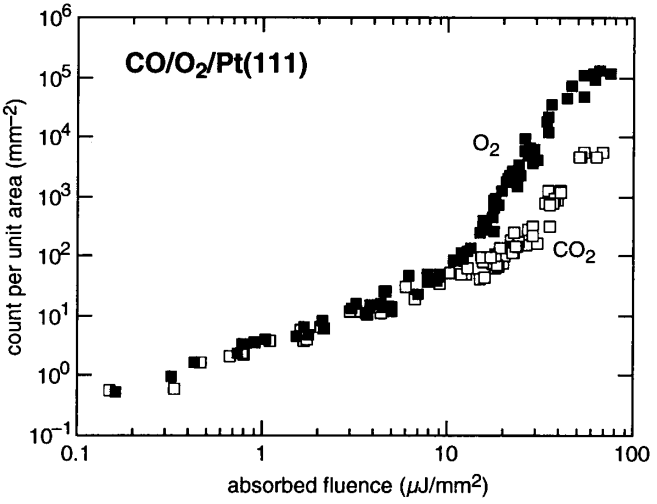

Figure X.6. Laser-induced (267-nm, 0.35-ps) yields of O_2, and CO_2 from $CO/O_2/Pt$. Each data point represents the yield from a fresh (not yet irradiated) spot on the platinum.

mechanical shutter, we reduce the laser repetition rate to 2 Hz to allow the gas-phase products to be pumped out of the chamber. The background levels, measured 50 ms before each laser pulse, do not change over the course of an experiment. The detection limit for each mass-to-charge ratio depends on the background present in the chamber at that mass and on the signal due to cracking of higher mass species in the mass spectrometer ionizer. Counts attributable to the background in the vacuum chamber have been subtracted from the data.

Figure X.6 shows the yields of O_2 and CO_2 from $CO/O_2/Pt(111)$. Each data point represents the yield from a single laser pulse at a new location on the platinum. The data are normalized to the laser spot size to allow comparison between data runs taken with different spot sizes. The figure shows a cross-over[49,62] near 10 $\mu J/mm^2$. Below this cross-over fluence the yield varies linearly with fluence; above the cross-over nonlinear contributions greatly enhance the yield. In this section we focus on data obtained in this nonlinear regime. We measured reaction yields for several combinations of reactants and isotopes to determine the reaction pathway in the nonlinear regime.

Table X.6 summarizes the yields from various surface preparations. The shading indicates the species deposited on the surface before irradiation. As can be seen in Fig. X.6, the ratio of the CO_2 and O_2 yields is constant between 30 and 80 $\mu J/mm^2$; for all

	CO	CO/O	CO/O_2		O_2/O_2	O_2/O	O
	1	2	3	4	5	6	7
^{18}O		<0.2[a]					<0.2[a]
$^{16}O_2$					80 ± 5	15 ± 5	
$^{18}O^{16}O$					0.5 ± 0.2	0.05 ± 0.02	
$^{18}O_2$		0 ± 0.001[b]	25 ± 5	25 ± 5	40 ± 10		0 ± 0.001[b]
$C^{16}O$							
$C^{18}O$	0.03 ± 0.01	0.5 ± 0.2	<0.2[c]				
$C^{16}O^{18}O$				1 ± 0.2			
$C^{18}O_2$	0 ± 0.001[b]	0.01 ± 0.005	1 ± 0.2	0.01[d]			

Table X.6: Relative yields due to nonlinear photochemistry for seven different surface preparations. The shading indicates which species were dosed to the surface. The numbers in the table indicate the relative yields of the various molecules and their isotopic variations, normalized to the yield of CO_2 from CO/O_2/Pt(111). Yields are reported for 267-nm, 0.35-ps laser pulses at a fluence of 30 $\mu J/mm^2$.

[a]signal attributed to water background signal

[b]detection limit

[c]signal attributed to cracking of CO_2

[d]signal attributed to isotopic impurity in surface preparation

sample preparations studied, the product ratios vary little over this fluence range. The branching ratio between O_2 desorption and CO_2 formation changes when passing from the linear to the nonlinear regime; O_2 desorption is the dominant pathway in the nonlinear regime. The values in the Table correspond to the laser-induced yields at a fluence of 30 $\mu J/mm^2$ and are normalized to the yield of $C^{18}O_2$ from $C^{18}O/^{18}O_2$/Pt(111). Where a maximum yield is given, the yield is below our detection limit for that species and sample preparation.

We first verified that there is no CO_2 production from a surface prepared with CO alone. As the data in column 1 of Table X.6 show, there is no measurable CO_2 yield within the detection limit. We do, however, observe a small CO yield.

Column 2 shows that, in contrast to experiments with low intensity irradiation,[1] some CO_2 is produced from reaction of carbon monoxide coadsorbed with oxygen atoms. We also observe CO desorption for this surface preparation. The oxygen, however, does not desorb as either atomic or molecular oxygen.

Columns 3 and 4 summarize yields from a surface preparation of carbon monoxide coadsorbed with oxygen molecules. We used $C^{18}O$ and $C^{16}O$ isotopes to see if the original oxygen atom in the CO gets replaced in the formation of CO_2. The yield of $C^{18}O_2$ reported in column 4 can be attributed to isotopic impurities in the surface preparation and thus we find no evidence for oxygen replacement in the CO_2 formation under subpicosecond laser irradiation.

The data in column 3 allow us to establish that the CO yield reported in columns 1 and 2 is not due to cracking of CO_2 in the mass spectrometer. In the experiments of column 3, the signal at 30 amu is 0.2 (20% of the CO_2 signal). This gives an upper limit of 20% for the probability of cracking of the laser-produced CO_2 in the ionizer. Thus in column 1, the maximum amount of signal at 30 amu that can be attributed to cracking of CO_2 is 20% of 0.01, which is well below the observed signal.

The experiments summarized in column 5 address whether there is exchange of oxygen atoms between $^{18}O_2$ and $^{16}O_2$ during laser-induced desorption from ($^{18}O_2$, $^{16}O_2$)/Pt(111). The observed yield of $^{16}O^{18}O$ is 240 times smaller than the yield of $^{18}O_2$ or $^{16}O_2$. We find therefore no evidence of atom exchange between oxygen molecules under subpicosecond laser irradiation.

In column 6 we investigate exchange of oxygen atoms between molecular $^{16}O_2$ and coadsorbed atomic ^{18}O. Again we obtain a yield of $^{16}O^{18}O$ that is much smaller than the yield of $^{16}O_2$. This result contrasts sharply with the observation of a reaction between oxygen atoms from the photodissociation of N_2O and coadsorbed oxygen atoms.[43]

Column 7 shows that there is no laser-induced recombination of atomic oxygen on the surface. As in the case of coadsorbed CO and O (column 2), there is no detectable desorption of atomic oxygen.

The small $C^{18}O_2$ and $^{16}O^{18}O$ yields in columns 4–6 of Table X.6 are due either to laser-induced processes or to isotopic impurities in the surface preparation. We therefore compared the laser-induced yields with thermal yields obtained by temperature programmed reaction spectroscopy. To determine the thermal yield of oxygen, we measured the areas under the α-peaks of the various isotopes of O_2 for ($^{18}O_2$,$^{16}O_2$)/Pt(111) and $^{16}O_2$/^{18}O/Pt(111) surface preparations. Thermal CO_2 yields were obtained by integrating the areas under corresponding CO_2 TPRS scans for a $C^{16}O$/$^{18}O_2$/Pt(111) sample preparation. The thermal yields are reported in Table X.7, labeled and normalized within each column for easy comparison to Table X.6. The $C^{18}O_2$ and $^{16}O^{18}O$ yields in Table X.6 are comparable to those in Table X.7. It is

	CO/O_2	O_2/O_2	O_2/O
	4	5	6
^{18}O			
$^{16}O_2$		80	15
$^{18}O^{16}O$		0.3	0.07
$^{18}O_2$		45	
$C^{16}O$			
$C^{18}O$			
$C^{16}O^{18}O$	1		
$C^{18}O_2$	0.01		

Table X.7: Summary of the relative thermal chemistry yields due to molecular mechanisms for various surface preparations. The shading indicates which species were dosed to the surface. The numbers in the table indicate the relative yields of the molecules and their isotopic variations. In column 4, the yields are normalized to the $C^{16}O^{18}O$ yield; in columns 5 and 6, the yields are normalized so that the $^{16}O_2$ yields match the corresponding values in Table X.6.

therefore likely that the small $C^{18}O_2$ and $^{16}O^{18}O$ yields reported in Tables X.1 and X.2 are due to isotopic impurities.

5.2 Test for dissociation

To determine if high-intensity subpicosecond laser pulses cause photodissociation of oxygen, we irradiated the entire surface of a saturated 0.44 ML $^{18}O_2$/Pt(111) preparation and then determined the remaining surface coverage with a post-irradiation[3] temperature programmed reaction scan. The lower trace in Fig. X.7 shows the temperature programmed reaction scan for $^{18}O_2$ following irradiation of the $^{18}O_2$/Pt(111) surface with 55 $\mu J/mm^2$, 800-nm pulses. We used 800-nm pulses because there is no linear photo-dissociation of O_2 at that wavelength.[20,29] Any photo-dissociation at 800 nm must therefore be due to the mechanism responsible for nonlinear chemistry. However, we observe no desorption of α-O_2 or β-O_2 (lower trace in Fig. X.7). This indicates that no detectable amount of oxygen molecules or oxygen atoms is left on the surface after irradiation.

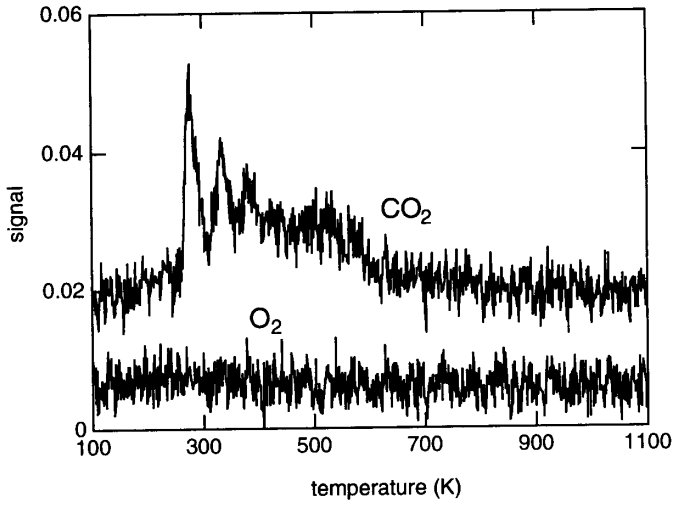

Figure X.7: Temperature programmed desorption of O_2/Pt(111) following irradiation with 800-nm, 55 μJ/mm^2 pulses.

Does this mean that the laser pulses do not dissociate the oxygen molecules? It is possible that the laser dissociates a small fraction of the O_2 molecules, and that the O atoms are scavenged by background gas molecules that adsorb to the surface. For example, if $C^{16}O$ adsorbs during the experiment, it could react with atomic ^{18}O created by the laser and prevent this oxygen atom from appearing as β-O_2 during the temperature programmed reaction scan. Figure X.7 shows a small amount of $C^{16}O^{18}O$. This very low CO_2 signal could be due to reaction on the sample mount. If, however, we attribute all of this signal to reaction between laser-dissociated oxygen and background contamination, we obtain an upper limit for laser-induced dissociation of 1.8% of the initial O_2 coverage.

5.3 Inferring reaction pathways

A number of different pathways can lead to the observed O_2 desorption and CO oxidation. Here we examine different possibilities in light of the data presented in the previous section.

Consider first an atomic pathway — oxidation of CO due to interaction with an oxygen atom:

$$O_2(ad) \rightarrow 2O^*(ad)$$
$$O^*(ad) + CO(ad) \rightarrow CO_2(g)$$

The observed ratio of CO_2 formation to O_2 desorption at 800 nm is 1:70 and so, if each time an oxygen molecule dissociates both atoms react with CO, then the ratio of O_2 dissociation to desorption must be about $1/140 \approx 0.7\%$. This is below the upper limit of 1.8% we established for the probability of O_2 dissociation and so we cannot rule out an atomic pathway even though such a pathway would require an efficiency of at least $0.7/1.8 \approx 40\%$ for the capture of the oxygen atoms by CO.

Dissociation of O_2 could also lead to other reactions. However, we observe no recombination of oxygen atoms back to O_2 (column 5, Table X.6) and no reaction of the dissociation fragments with coadsorbed oxygen atoms (column 6, Table X.6). So, if dissociation occurs, we must conclude that the fragments of oxygen dissociated with subpicosecond laser pulses do not react with other oxygen atoms or molecules, in sharp contrast to the oxygen atom formed in the photodissociation of N_2O.[43]

Next we consider a molecular pathway — CO oxidation by direct interaction with an oxygen molecule:

$$O_2(ad) \rightarrow O_2^*(ad)$$
$$O_2^*(ad) + CO(ad) \rightarrow CO_3^*(ad) \rightarrow O(ad) + CO_2(g)$$

In this scheme, the carbon dioxide is produced not via dissociation of oxygen but through a CO_3 intermediate. A stable CO_3 species has been observed on Ag(110),[70] but has not been reported on Pt(111). In fact, we observe no exchange of the oxygen atom originating on the CO molecule to better than 1 part in 100 (column 4, Table X.6). Therefore, if CO is oxidized by the molecular pathway, the oxygen atoms of the CO_3^* intermediate must be highly inequivalent and the intermediate is constrained to dissociate into CO_2 and O without eliminating the oxygen initially present on the CO.

It is also possible that the reaction between the oxygen molecule and the carbon monoxide occurs in a concerted process in which O_2 and CO interact so that the O–O bond is stretched as the new O–CO bond is formed.

Let us next turn to the desorption of oxygen. Suppose the oxygen molecules dissociate and atomic oxygen then recombines to give O_2:

$$O_2(ad) \rightarrow 2O^*(ad)$$
$$2O^*(ad) \rightarrow O_2(g)$$

Such a pathway must lead to mixing of oxygen isotopes in the ($^{16}O_2$, $^{18}O_2$)/Pt(111), which is not observed experimentally (column 5, Table X.6). Furthermore, if they fail to recombine, the oxygen atoms should equilibrate with the surface. However, we observe very few oxygen atoms in the post-irradiation temperature programmed desorption experiments (see Section 5.2). This observation also excludes the possibility[37] that oxygen desorption is caused by displacement due to nearby chemisorption of atomic oxygen. Our observations therefore show that the observed O_2 products are due to desorption of intact molecules.

5.4 Summary

Our results show that the oxygen molecules desorb from O_2/Pt(111) without exchange of oxygen atoms between molecules, analogous to the α-O_2 product in thermal chemistry. We observe no yield of O_2 from O/Pt(111) nor from a reaction between a fragment of O_2 and a coadsorbed, equilibrated oxygen atom in O_2/O/Pt(111).

While we cannot conclusively attribute CO_2 production to either an atomic or a molecular pathway, our results allow us to put constraints on both pathways. If the molecular pathway is operative, then the isotope exchange experiments show that the CO_3* intermediate has very inequivalent oxygen atoms. If the CO oxidizes by the atomic pathway, then the capture of oxygen atoms by the carbon monoxide must be highly efficient.

6. Conclusion

In this paper we reviewed recent developments in the photochemistry of oxygen on platinum. Though reactions of oxygen on platinum are of particular interest because of their practical importance, many of the issues relevant to this system are being explored for a wide range of adsorbates and substrates.

It is clear that the metal substrate is essential to the photochemistry. In linear photochemistry, the substrate mediates the reaction either directly or indirectly. In nonlinear surface femtochemistry, the high density of excited substrate electrons leads to high cross sections for desorption and reaction. Through a combination of modeling and experiments a number of scenarios have been developed to describe the

transfer of energy from the excited substrate electrons to nuclear motion of the adsorbates.

An aim of current research in surface chemistry is to determine the nature of the reactive species in a surface reaction. The experiments presented here begin to address this question for a surface reaction stimulated with subpicosecond laser pulses. The field of surface femtochemistry is a new and challenging branch of femtochemistry. As more groups focus their efforts in this area, we can look forward to many exciting new developments.

7. Acknowledgments

We wish to thank Professors Cynthia M. Friend and Eric J. Heller for many useful discussions. This work was supported by the Army Research Office grants DAAH04-95-0615 and DAAH04-95-0370. RJF wishes to acknowledge a scholarship from the Natural Science and Engineering Research Council of Canada.

References

1 W. D. Mieher and W. Ho, *J. Chem. Phys.* **91,** 2755-2756 (1989).
2 J. M. White, *J. Vac. Sci. Technol. B* **10,** 191-195 (1992).
3 J. A. Misewich, T. F. Heinz, P. Weigand, and A. Kalamarides, in *Laser spectroscopy and photochemistry on metal surfaces Part II*, Vol. 5, edited by H.-L. Dai and W. Ho (World Scientific, Singapore, 1995).
4 J. A. Prybyla, T. F. Heinz, J. A. Misewich, M. M. T. Loy, and J. H. Glownia, *Phys. Rev. Lett.* **64,** 1537-1540 (1990).
5 *Laser spectroscopy and photochemistry on metal surfaces Part II*, Vol. 5, edited by H.-L. Dai and W. Ho (World Scientific, Singapore, 1995).
6 W. Ho, *Comm. Cond. Mat. Phys.* **13,** 293-327 (1988).
7 W. Ho, *Surf. Sci.* **299/300,** 996-1007 (1994).
8 X.-Y. Zhu, *Annu. Rev. Phys. Chem.* **45,** 113-144 (1994).
9 W. Ho, *Surf. Sci.* **363,** 166-178 (1996).
10 R. R. Cavanagh, D. S. King, J. C. Stephenson, and T. F. Heinz, *J. Phys. Chem.* **97,** 786-798 (1993).
11 J. Grimblot, A. C. Luntz, and D. E. Fowler, *Journal of electron spectroscopy and related phenomena* **52,** 161-174 (1990).

12 H. Steininger, S. Lehwald, and H. Ibach, *Surface Science* **123,** 1-17 (1982).
13 M. Orchin and H. H. Jaffé, *Symmetry, Orbitals, and Spectra (S.O.S.)* (Wiley-Interscience, New York, 1971).
14 W. Wurth, J. Stöhr, P. Feulner, X. Pan, K. R. Bauchspiess, Y. Baba, E. Hudel, G. Rocker, and D. Menzel, *Phys. Rev. Lett.* **65,** 2426-2429 (1990).
15 W. Eberhardt, T. H. Upton, S. Cramm, and L. Incoccia, *J. Vac. Sci. Tech. A* **6,** 876-877 (1988).
16 D. A. Outka, J. Stöhr, W. Jark, P. Stevens, J. Solomon, and R. J. Madix, *Phys. Rev. B* **35,** 4119-4122 (1987).
17 A. W. E. Chan, R. Hoffmann, and W. Ho, *Langmuir* **8,** 1111-1119 (1992).
18 B. Hellsing, *Surf. Sci.* **282,** 216-228 (1993).
19 I. Panas and P. Siegbahn, *Chem. Phys. Lett.* **153,** 458-464 (1988).
20 W. D. Mieher and W. Ho, *J. Chem. Phys.* **99,** 9279-9295 (1993).
21 J. Gland, V. Secton, and G. Fisher, *Surface Science* **95,** 587-602 (1980).
22 N. Avery, *Chem. Phys. Lett.* **96,** 371-373 (1983).
23 L. Vaska, *Acc. Chem. Res.* **9,** 175-183 (1976).
24 N. V. Smith, *Phys. Rev. B* **9,** 1365 (1974).
25 K. Mortensen, C. Klink, F. Jensen, F. Besenbacher, and I. Stensgaard, *Surface Science* **220,** L701-L708 (1989).
26 K. Sawabe and Y. Matsumoto, *Chem. Phys. Lett.* **194,** 45-50 (1992).
27 T. Matsushima, *Surface Science* **127,** 403-423 (1983).
28 S. Deliwala, R. J. Finlay, J. R. Goldman, T. H. Her, W. D. Mieher, and E. Mazur, *Chem. Phys. Lett.* **242,** 617-622 (1995).
29 X.-Y. Zhu, S. R. Hatch, A. Campion, and J. M. White, *J. Chem. Phys.* **91,** 5011-5020 (1989).
30 C. E. Tripa, C. R. Arumaninayagam, and J. T. Yates, *J. Chem. Phys.* **105,** 1691-1696 (1996).
31 F.-J. Kao, D. G. Busch, D. G. d. Costa, and W. Ho, *Phys. Rev. Lett* **70,** 4098-4101 (1993).
32 V. A. Ukraintsev and I. Harrison, *J. Chem. Phys.* **96,** 6307-6310 (1992).
33 L. J. Richter, S. A. Buntin, D. S. King, and R. R. Cavanagh, *Chem. Phys. Lett.* **186,** 423-426 (1991).
34 J. D. Jackson, *Classical Electrodynamics*, Second Edition ed. (John Wiley and Sons, New York, 1962).
35 F. Weik, A. deMeijere, and E. Hasselbrink, *J. Chem. Phys.* **99,** 682-694 (1993).
36 S. R. Hatch, X.-Y. Zhu, J. M. White, and A. Campion, *J. Phys. Chem.* **95,** 1759-1768 (1991).

37 C. T. Rettner and J. Lee, *J. Chem. Phys.* **101,** 10185-10188 (1994).
38 H. Hirayama, A. d. Meijere, and E. Hasselbrink, *Surf. Sci.* **287/288,** 160-164 (1993).
39 C. Åkerlund, I. Zoric, J. Hall, and B. Kasemo, *Surf. Sci.* **316,** L1099-L1104 (1994).
40 K.-H. Allers, H. Pfnür, P. Feulner, and D. Menzel, *J. Chem. Phys.* **100,** 3985-3998 (1994).
41 J. Gland and E. Kollin, *J. Chem. Phys.* **78,** 963-974 (1983).
42 T. A. Germer and W. Ho, *J. Chem. Phys.* **93,** 1474-1475 (1990).
43 K. Sawabe, J. Lee, and Y. Matsumoto, *J. Chem. Phys.* **99,** 3143-3146 (1993).
44 A. N. Artsyukhovich and I. Harrison, *Surface Science* **350,** L199-L204 (1996).
45 J. Kiss and J. M. White, *J. Phys. Chem.* **95,** 7852-7857 (1991).
46 F. Budde, T. F. Heinz, A. Kalamarides, M. M. T. Loy, and J. A. Misewich, *Surf. Sci.* **283,** 143-157 (1993).
47 J. A. Prybyla, H. W. K. Tom, and G. D. Aumiller, *Phys. Rev. Lett.* **68,** 503-506 (1992).
48 L. M. Struck, L. J. Richter, S. A. Buntin, R. R. Cavanagh, and J. C. Stephenson, *Phys. Rev. Lett.* **77,** 4576-4579 (1996).
49 R. J. Finlay, S. Deliwala, J. R. Goldman, T. H. Her, W. D. Mieher, C. Wu, and E. Mazur, in *SPIE Proceedings*, Vol. 2547 (1995), pp. 218-226.
50 J. A. Misewich, A. Kalamarides, T. F. Heinz, U. Höfer, and M. M. T. Loy, *J. Chem. Phys.* **100,** 736-739 (1994).
51 F. Budde, T. F. Heinz, M. M. T. Loy, J. A. Misewich, F. d. Rougemont, and H. Zacharias, *Phys. Rev. Lett.* **66,** 3024-3027 (1991).
52 F.-J. Kao, D. G. Busch, D. Cohen, D. G. d. Costa, and W. Ho, *Phys. Rev. Lett.* **71,** 2094-2097 (1993).
53 S. I. Anisimov, B. L. Kapeliovich, and T. L. Perel'man, *Sov. Phys. JETP* **39,** 375 (1974).
54 R. W. Schoenlein, W. Z. Lin, and J. G. Fujimoto, *Phys. Rev. Lett.* **58,** 1680-1683 (1987).
55 X. Y. Wang, D. M. Riffe, Y.-S. Lee, and M. C. Downer, *Phys. Rev. B* **50,** 8016-8019 (1994).
56 P. A. Redhead, *Can. J. Phys.* **42,** 886-905 (1964).
57 D. Menzel and R. Gomer, *J. Chem. Phys.* **41,** 3311 (1964).
58 P. R. Antoniewicz, *Phys. Rev. B* **21,** 3811-3815 (1980).
59 J. A. Misewich, T. F. Heinz, and D. M. Newns, *Phys. Rev. Lett.* **68,** 3737-3740 (1992).

60 P. Avouris and R. E. Walkup, *Ann. Rev. Phys. Chem.* **40,** 173 (1989).
61 C. Springer and M. Head-Gordon, *Chem. Phys.* **205,** 73-89 (1996).
62 D. G. Busch and W. Ho, *Phys. Rev. Lett.* **77,** 1338-1341 (1996).
63 W. S. Fann, R. Storz, H. W. K. Tom, and J. Bokor, *Phys. Rev. B* **46,** 13592-13595 (1992).
64 W. S. Fann, R. Storz, H. W. K. Tom, and J. Bokor, *Phys. Rev. Lett.* **68,** 2834-2837 (1992).
65 W. S. Fann, R. Storz, H. W. K. Tom, and J. Bokor, *Surf. Sci.* **283,** 221-225 (1993).
66 S. M. Harris, S. Holloway, and G. R. Darling, *J. Chem. Phys.* **102,** 8235-8248 (1995).
67 C. Suárez, W. E. Bron, and T. Juhasz, *Phys. Rev. Lett.* **75,** 4536-4539 (1995).
68 R. G. Musket, W. McLean, C. A. Colmenares, D. M. Makowiecki, and W. J. Siekhaus, *Applications of Surf. Sci.* **10,** 143-207 (1982).
69 E. P. Ippen and C. V. Shank, *Appl. Phys. Lett.* **27,** 488-??? (1975).
70 E. M. Stuve, R. J. Madix, and B. A. Sexton, *Chem. Phys. Lett.* **89,** 48-53 (1982).